Interannual modulation of subthermocline eddy kinetic energy east of the Philippines

Yuchao Hui[1,3], Linlin Zhang[1,2,4], Zhenxiao Wang[1,3], Fan Wang[1,2,4], Dunxin Hu[1,2,4]

[1] Key Laboratory of Ocean Circulation and Waves, Institute of Oceanology, Chinese Academy of Sciences, Qingdao, China

[2] Pilot National Laboratory for Marine Science and Technology (Qingdao), Qingdao, China

[3] University of Chinese Academy of Sciences, Beijing, China

[4] Center for Ocean Mega-Science, Chinese Academy of Sciences, Qingdao, China

Corresponding author: Linlin Zhang (zhanglinlin@qdio.ac.cn)

Key points

- Significant interannual variation of subthermocline EKE related to ENSO is detected east of the Philippines
- Both barotropic and baroclinic instability are responsible for the interannual variation of EKE, and barotropic instability is dominant
- Interannual modulation of barotropic instability is associated with the variation of Mindanao Undercurrent and Halmahera Eddy

Abstract

Interannual variation of subthermocline eddy kinetic energy (EKE) east of the Philippines is investigated based on mooring measurements during 2015-2019 and ocean state estimates during 1995-2017 from the Oceanic General Circulation Model for the Earth Simulator (OFES). Prominent interannual variation of EKE is detected below the thermocline east of the Philippine coast, which is closely related to the El Niño and Southern Oscillation (ENSO) events and generally lags the Nino3.4 index by 14 months. Further energy diagnostic analysis indicates that the interannual variation of subthermocline EKE is controlled by both baroclinic and barotropic instability of the background flows and dominated by the barotropic instability especially. Barotropic instability in the southern part of the Philippine coast is associated with the subsurface component of the quasi-permanent anticyclonic eddy Halmahera Eddy (HE), while that in the northern part is closely related to the Mindanao Undercurrent (MUC). Both HE and MUC are modulated by the ENSO events. When El Niño occurs, negative sea surface height anomalies appear near the dateline and propagate westward in the form of the first mode baroclinic Rossby wave, exerting delayed impacts upon the western boundary currents east of the Philippine coast and further modulating the interannual variation of subthermocline EKE. Moreover, the barotropic energy conversion rate and its corresponding subthermocline EKE at lower latitudes responds relatively faster to ENSO due to the higher Rossby wave phase speed there.

Plain Language Summary

Subthermocline meso-scale eddies with maximum velocity below the thermocline are distributed widely over the world oceans and play a crucial role in the transport of subsurface

waters. The region east of the Philippine coast is featured with energetic eddies and high EKE in the subsurface layer. These eddies are intrinsic to the ocean, and extract energy from the mean potential energy and mean kinetic energy of the background currents. Based on 4-year mooring measurements and OFES outputs during 1995-2017, strong interannual variation of subthermocline EKE is detected in this region. Further analysis demonstrates that this interannual variation is mainly modulated by the evolution of barotropic instability, which is associated with the background flows of MUC and HE east of the Philippine coast. Additionally, the interannual variation of subthermocline EKE seems to be influenced by ENSO. The wind stress curl anomaly associated with El Niño events excites negative sea surface anomaly (SSHA) near the dateline, and the SSHA propagates westward in the first mode Rossby waves, producing delayed impacts on the western boundary currents and then on the variation of subthermocline EKE. This work enriches our knowledge of the low-frequency modulation of subthermocline EKE in this region.

Keywords

subthermocline EKE; interannual variation; western tropical Pacific; baroclinic\barotropic instability

1. Introduction

Meso-scale eddies are ubiquitous in the global ocean, which play crucial roles in modulating the variability of ocean currents, the cycle of material and energy, and even the climate change (e.g., Stammer 1998; Fu 2009; Chelton et al. 2011a). Generally, mesoscale eddies can be divided into two categories: surface-intensified eddy that has maximum velocity core in the upper layer and is

easily captured by sea surface features (e.g. Chelton et al. 2011b; Faghmous et al. 2015), and subthermocline eddy that mainly exists below the thermocline and shows very weak or even no signals at the sea surface (e.g. Mc Williams, 1985; Assassi et al., 2016). Due to the difficulty in observing, there are relatively few studies on subthermocline eddies. These limited studies indicate that subthermocline eddies are distributed widely over the world oceans and play an essential role in the transport of water mass below the thermocline (e.g. Simpson and Lynn 1990; Shapiro and Meschanov 1991; Richardson et al. 2000; Johnson and McTaggart 2010; Chiang et al. 2015; Nan et al. 2017).

The western tropical Pacific is the 'crossroad' of currents from the northern and southern hemispheres, and is featured with a complex three-dimensional circulation system. In the upper layer, North Equatorial Current (NEC) flows westward and bifurcates into northward Kuroshio and southward Mindanao Current (MC) when impinging at the Philippine coast at about 14ºN (e.g. Nitani 1972; Toole et al. 1990; Lukas et al. 1996; Hu et al. 2015). Further south, the main body of MC that turns to the east combines with the New Guinea Coastal Current/Undercurrent (NGCC/NGCUC) forming the source region of eastward-flowing North Equatorial Counter Current (NECC) (Lukas et al. 1991). Below the surface circulation system, opposite subsurface undercurrents appear, such as the Mindanao Undercurrent (MUC), Luzon Undercurrent (LUC), North Equatorial Undercurrent (NEUC), and North Equatorial Subsurface Current (NESC) (Fig. 1; e.g., Hu and Cui 1989; Yuan et al. 2014; Qiu et al. 2013; Wang et al., 2015; Hu et al. 2020).

The complicated surface and subsurface current system in the western tropical Pacific provide advantageous conditions for the generation of subthermocline eddies. Early hydrographic observations have shown the hints of subthermocline eddies existing east of the Philippine coast

(e.g., Firing et al., 2005; Dutrieux 2009). Recent enhanced mooring measurements also reveal significant intraseasonal variations of velocity with a period of 60-120 days centering below the thermocline, and these intraseasonal signals are attributed to the activity of subthermocline eddies (e.g., Zhang et al. 2014; Wang et al. 2014). Meanwhile, investigations based on model outputs demonstrate that abundant subthermocline eddies and high eddy kinetic energy (EKE) appear in this region (Fig. 2; e.g., Qu et al. 2012; Chiang and Qu, 2013; Xu et al. 2019). These eddies are believed to be intrinsic to the ocean, and both barotropic and baroclinic instability are important in the generation of these eddies (Dutrieux 2009; Chiang and Qu 2013; Wang et al. 2014; Chiang et al. 2015).

However, due to the lack of long-time observations focusing on subthermocline eddies in this region, most of previous studies tend to concentrate on the statistical characteristics, and only a few studies pay attention to the temporal variation of subthermocline eddies and their associated EKE. Based on 4 years of mooring observations and OFES outputs, Zhang et al. (2021) reveals the seasonal cycle of subthermocline EKE east of the Philippine coast. On the interannual time scale, basin-wide wind stress anomalies associated with El Niño and Southern Oscillation (ENSO) significantly modulate the variation of currents in the western Pacific through Ekman and Rossby wave dynamics (e.g., Kashino et al. 2009; Hsin and Qiu 2012; Qiu and Chen 2010; Ren et al. 2020). Given meso-scale eddies mainly extract energy from background flows, the interannual variation of the currents will potentially influence the variation of subthermocline EKE. Therefore, as a continuation of Zhang et al. (2021), this work is aimed to explore the interannual variation of subthermocline EKE east of the Philippine coast with 4 years of mooring measurements and long-term model outputs, and clarify the underlying mechanism and its

116 relationship with ENSO.

117 The rest of the paper is organized as follows. The data and method are presented in Section 2.
118 The interannual variation of subthermocline EKE is described in Section 3. Section 4 shows the
119 governing process of interannual variation of subthermocline EKE. The relationship between
120 subthermocline EKE and ENSO is discussed in Section 5. The conclusion is drawn in Section 6.

121

122 **2. Data and Methodology**

123 **2.1 Data**

124 a. OFES model outputs

125 The interannual variation of subthermocline EKE east of the Philippine coast is investigated
126 based on outputs from the Oceanic General Circulation Model for the Earth Simulator (OFES).
127 The OFES model is based on the third version of the Modular Ocean Model (MOM 3.0) that
128 covers a quasi-global ocean extending from 75ºS to 75ºN and has a horizontal resolution of 0.1º
129 and 54 vertical levels. The model is first initialized with the World Ocean Atlas 1998 (WOA98)
130 and spun up for 50 years. Driven by different climatological monthly fields, the model produces
131 three types of simulation products, i.e., OFES-CLIM product, which is forced by the same
132 climatological monthly fields of NCEP; OFES-NCEP product, which is integrated from 1950
133 using daily surface wind stress, heat flux, and salinity flux forcing provided by NCEP; and
134 OFES-QSCAT product, which is forced by the wind stress data of the QuikSCAT measurements
135 from 22 July 1999 to 30 October 2009. In this work, the OFES-NCEP outputs with a 3-day
136 snapshot from 1995 to 2017 are used. Detailed descriptions of this model can be found in
137 Masumoto et al. (2004) and Sasaki et al. (2008).

OFES outputs have been widely applied to the investigation of the general circulation and meso-scale eddies in the western Pacific, and these studies indicate that the model outputs are generally consistent with different types of observations (e.g., Dutrieux 2009; Wang et al 2014; Chiang and Qu 2013; Song et al. 2017; Zhang et al. 2021). For instance, Song et al. (2017) has compared the climatological mean circulation simulated by OFES with the World Ocean Atlas 2013 and indicates that the model outputs roughly agree with observations in both the upper and intermediate layers. Chiang and Qu (2013) reveal a good consistency between the OFES-simulated velocity and mooring observations at 2.5ºS, 142ºE on the seasonal time scale. Zhang et al. (2021) further compares the modeled subthermocline EKE with three mooring observations east of the Philippines and suggests that the model outputs well capture the seasonal variability of subthermocline EKE recorded by mooring observations. Therefore, we believe that OFES is one of the most suitable model products to explore the ocean currents and meso-scale eddies in the western tropical Pacific.

b. Mooring measurements

Two subsurface moorings were deployed at 8.5ºN, 130ºE from 26th September 2015 to 24th October 2019 and 12.5ºE, 130ºN from 26th December 2016 to 30th November 2018, respectively. One upward-looking and one downward-looking ADCPs were mounted on the main float at 450 m for each mooring, which collected nearly 4-year and 2-year velocity data in the upper 900 m, respectively. The original hourly data is daily averaged to remove the tidal influence and then interpolated onto the standard pressure levels from 50 m to 900 m with the vertical interval of 10 m. These two moorings are maintained every year to recover data and replace batteries. Due to technical problems, the velocity data at 8.5ºN, 130ºE from 21th September 2018 to 6th December

2018 is unavailable. For detailed configuration of the ADCPs, see Zhang et al. (2014).

c. Sea Surface Height

The monthly gridded and merged absolute dynamic topography in the tropical Pacific, with a horizontal resolution of 0.25º×0.25º for the period of 1995-2017 is also used in this study. This dataset is provided by Aviso+ (http://www.aviso.altimetry.fr) and distributed by Copernicus Marine Environment Monitoring Service (CMEMS, http://marine.copernicus.eu/).

2.2 Calculations of EKE and barotropic/baroclinic conversion rate

Previous studies reveal that the dominant periods of subthermocline eddies east of the Philippine coast are about 60-120 days (Qu et al. 2012; Zhang et al. 2014). Therefore, a 150-day high-pass filter is applied to the original velocity data to isolate subthermocline eddy signals, and the 150-day low-pass filtered velocity fields are regarded as the low-frequency varying background flow, as shown in formula (1).

$$u(x,y,t) = \tilde{u}(x,y,t) + u'(x,y,t) \qquad (1)$$

$\tilde{u}$ and u' denote the velocity signals with time scales longer and shorter than 150 days, respectively. u' is also used to calculate the EKE with formula (2).

$$EKE = \frac{1}{2}(u'^2 + v'^2) \qquad (2)$$

The barotropic energy conversion rate (BTR) and baroclinic energy conversion rate (BCR) are usually used to quantify the barotropic and baroclinic instability of the background currents. Positive BTR denotes the transportation of energy from the mean kinetic energy to EKE, and positive BCR means that mesoscale eddies extract energy from the mean available potential energy of the background currents. Many previous studies have revealed the significance of

background instability on the generation of subthermocline eddies in the western Pacific (e.g. Wang et al. 2014; Chiang et al. 2015; Qiu et al. 2015). Thus, BTR and BCR are calculated in this study according to formula (3) and (4).

$$BTR = -[\underbrace{u'u'\frac{\partial \tilde{u}}{\partial x} + u'v'\frac{\partial \tilde{u}}{\partial y}}_{u\text{-}term} + \underbrace{u'v'\frac{\partial \tilde{v}}{\partial x} + v'v'\frac{\partial \tilde{v}}{\partial y}}_{v\text{-}term}] \quad (3)$$

$$BCR = \left(\frac{g}{\rho_0}\rho' w'\right) \quad (4)$$

ρ' and w' in formula (4) indicate the 150-day high-pass filtered potential density and vertical velocity, while g and ρ_0 are the gravity constant and background potential density with the value of 9.807 m/s^2 and 1025 kg/m^3, respectively.

3. Interannual variation of subthermocline EKE

One of the most pronounced characteristics in the ocean circulation east of the Philippine coast is the energetic eddy activities and high EKE in the subsurface layer (Fig. 2; e.g., Qu et al. 2012; Chiang et al. 2015). Measurements from two subsurface moorings in this region indicate that the subthermocline EKE exhibits distinguished interannual fluctuations (Fig. 3). Elevated subthermocline EKE exists during March to June of 2016 and April to June of 2019, and quite weak subthermocline EKE appears during July 2017 to July 2018 at 8.5ºN, 130ºE (Fig. 3a). Similar phenomenon is also shown at 12.5ºN, 130ºE with strong signals during January to February of 2017 and weak signals during the rest of the observation period (Fig. 3b). To better understand the interannual variation of subthermocline EKE in this area, OFES outputs will be used in the following analysis because mooring observations only provide information at a few sporadic sites. The 3-day subthermocline EKE derived from OFES outputs during 1995-2017 is

first averaged into monthly time series, and then an empirical orthogonal function (EOF) analysis is applied to the monthly EKE. Here, 300-700 m is chosen as the subthermocline layer in the calculation of EKE considering the energetic subthermocline eddy activities in this depth range (Fig. 2b; Zhang et al. 2021).

Figure 4 shows the first two leading EOF modes and their corresponding time series. The first EOF mode captures 15 % of the total variance and exhibits a nearly in-phase EKE variation in the whole study area, except for a minor inconsistency southeast of Mindanao Island. The signals are mainly concentrated near the western boundary, consistent with the distribution of subthermocline EKE shown in Fig. 2a. The PC1 (primary component) time series almost coincides with the interannual variation of regional mean subthermocline EKE with their correlation of 0.89 (Fig. 4c). Here, the regional mean subthermocline EKE is averaged in the black box (5º-14ºN, 125º-130ºE) shown in Figure 4a. Therefore, the first EOF mode reveals the variation of subthermocline EKE on the interannual time scale. The second EOF mode accounts for 7.2 % of the total variance and exhibits a dipole-like structure of EKE separated by 10ºN. The PC2 time series demonstrates obvious seasonal cycle with peaks in summer and troughs in winter for most of the years. To further confirm this seasonal cycle, a power spectral analysis is applied to PC2, and the spectrum of PC2 peaks at the period of 1 year, which is statistically significant at the 95 % confidence level (not shown). It suggests that the second EOF mode captures the seasonal cycle of subthermocline EKE east of the Philippine coast, agreeing with Zhang et al. (2021). In addition, the first EOF mode (15.0 %) is beyond double of the proportion of variance of the second mode (7.2%), implying the dominant role of the interannual variation of subthermocline EKE in this region.

The interannual variation of subthermocline EKE is further compared with the normalized Nino 3.4 index after 1-year running mean from NOAA Earth System Research Laboratory. Time series of regional mean subthermocline EKE shows elevated value during 1997-1998, 2003-2004, 2007-2008, 2010-2011, and 2016-2017, which is closely related to the ENSO events (Fig. 4c). Figure 5 shows the lead-lag correlation between the regional mean subthermocline EKE and Nino 3.4 index, and the correlation reaches 0.49 when ENSO leads by 14 months. Checked case by case, almost every El Niño event is followed by an elevation of subthermocline EKE. Therefore, the interannual variation of the subthermocline EKE seems to be modulated by ENSO.

Zhang et al. (2021) has reported opposite seasonal cycle of subthermocline EKE at different latitude bands in this region, and we therefore check the interannual variation of subthermocline EKE at different latitudes and their correlation with ENSO (Fig. 6). In general, the EKE at the lower latitude bands lags ENSO by relatively shorter period, and the lagging time varies from about 8 months at lower latitudes to about 16 months at higher latitudes. This lag correlation is also confirmed by two mooring observations at 8.5ºN, 130ºE and 12.5ºN, 130ºE. As shown in Figure 3, when the El Niño occurs during 2015-2016, significant subthermocline EKE firstly appears at 8.5ºN, 130ºE after about 7 months, then the mooring at 12.5ºN, 130ºE observes elevated EKE after about 15 months. Moreover, the nearly 4 years of mooring observations at 8.5ºN, 130ºE cover two El Niño events, i.e., 15/16 and 18/19 El Niño, and during the second El Niño cycle, the same lag correlation is also detected with EKE lagging El Niño by 6 months. In addition, Nan et al. (2019) also observes elevated subthermocline eddy activities during June-July of 2016 by a mooring system at 8ºN, 129ºE, which exactly lags the 15/16 El Niño by

7-8 months. Above all, multiple mooring measurements suggest that the interannual variation of subthermocline EKE in this region lags the ENSO events by several months.

4. Governing process of the interannual variation of subthermocline EKE

4.1 Barotropic and baroclinic energy conversion

Generally speaking, meso-scale eddies could be generated through either external forcing or internal instability of background flows. Based on different types of model outputs, Dutrieux (2009) suggests that the intermediate meso-scale eddies east of the Philippine coast are intrinsic to the ocean, mainly sourced from mixed vertical and horizontal instability of the local background flows. Besides, many other previous studies also emphasized the essential role of background flow instability in the generation of subsurface meso-scale eddies in this region (e.g. Wang et al. 2014; Chen et al. 2015; Chiang et al. 2015; Zhang et al. 2021). Therefore, both barotropic and baroclinic energy conversion rates (BTR and BCR) are calculated with OFES data. Figure 7a shows the interannual variation of regional mean subthermocline EKE and the sum of BTR and BCR in the black box east of the Philippine coast (5º-14º, 125º-130ºE; Fig. 2a). The regional mean BTR plus BCR matches well with the subthermocline EKE and leads the EKE by 4 months with a correlation of 0.78, statistically significant at 95 % confidence level (Fig. 7c). This 4-month lag reflects the ocean's internal adjustment period. Similar lead-lag correlations between the flow instability and EKE are also found in the NEC/STCC region (e.g., Qiu 1999).

To further quantify the contributions of barotropic and baroclinic instability to the interannual variation of subthermocline EKE, the time series of regional mean subthermocline BTR and BCR are shown in Figure 7b. In terms of the mean state, the averaged value of BCR is 1.55×10^{-9}

m^2/s^3, almost twice as much as that of BTR which is 0.89×10^{-9} m^2/s^3. It suggests that subthermocline meso-scale eddies could extract energy from both baroclinic and barotropic instability of the background flows, and the baroclinic process is dominant. Although the mean value of BCR is larger than that of BTR, the interannual variation of subthermocline EKE seems to be mainly controlled by BTR except for 2003. The standard deviation of BTR is 0.71×10^{-9} m^2/s^3, larger than that of BCR of 0.54×10^{-9} m^2/s^3 (exclude 2003), implying the dominant role of barotropic instability. Meanwhile, almost every peak in the time series of BTR coincides with the elevated EKE, for example, during 1997, 1999, 2007-2008, 2010-2011, and 2015-2016 (Fig.7a and 7b). Therefore, we suggest that the interannual variation of subthermocline EKE is mainly modulated by the evolution of barotropic instability of the background flows, while the baroclinic instability also plays important role in it.

It is worth noting that Figure 6 demonstrates the significant lag correlation between the subthermocline EKE and ENSO, and two correlation maxima with value exceeding 0.5 appear near 7ºN and 12ºN, separated by a correlation minimum at 9ºN. This characteristic suggests that there may be different processes controlling the interannual modulation of subthermocline EKE in the northern and southern parts of the region along the Philippine coast. Therefore, the study region is separated into the northern part (125º-130ºE, 9º-14ºN) named Box 1 and southern part (125º-130ºE, 5º-9ºN) named Box 2 (Fig. 4a). The interannual variation of regional mean subthermocline EKE and corresponding BTR/BCR in Box 1 and Box 2 are shown in Figure 8. In Box 2, the mean value of BTR is 2.16×10^{-9} m^2/s^3, significantly larger than that of BCR which is 0.90×10^{-9} m^2/s^3. Meanwhile, the prominent interannual fluctuation of BTR is detected with a standard deviation of 1.55×10^{-9} m^2/s^3, which is highly correlated with the interannual variation of

subthermocline EKE (Fig. 8b). While the variation of BCR on the interannual time scale is relatively indistinctive with a standard deviation of 0.67×10^{-9} m^2/s^3, and its relationship with the subthermocline EKE is ambiguous as well. In Box 1, although the mean value of BCR (2.03×10^{-9} m^2/s^3) is larger than that of BTR (nearly 0), the interannual variation of BTR is almost coherent with the subthermocline EKE except in 2003 (Fig. 8a), and the BTR exhibits distinguished peaks when enhanced subthermocline EKE appears. In hence, the evolution of barotropic instability is the primary reason for the interannual modulation of subthermocline EKE in both Box 1 and Box 2. As for 2003, the elevated subthermocline EKE seems due to the baroclinic instability (Fig. 8a). There is no La Niña occurring after the 02/03 El Niño event, and this abnormal ENSO cycle may be responsible for the elevated EKE in 2003. Detailed physical processes on this issue will be explored in future studies.

4.2 Source of barotropic instability

According to formula (3), the BTR consists of two components which are associated with the horizontal derivative of zonal and meridional background flow. We use u-term and v-term to represent the two components of BTR, and further identify the dominant term. Figure 9 shows the horizontal distribution of climatological mean subthermocline BTR and its two components. In the mean BTR, significant signal appears near the western boundary region, especially east of Mindanao where two positive BTR bands exist nearly parallel to the coast (Fig. 9a), which is similar to the distribution of subthermocline EKE (Fig. 2a). Same as the horizontal distribution of BTR, signals in the u-term and v-term also concentrate in the western boundary region. Negative values are dominant in the u-term, with only several positive spots existing sporadically to the

313 east of the Mindanao coast (Fig. 9b). While the v-term is featured with an opposite spatial pattern
314 to that of u-term, with a 2º-width positive jet locating north of 8ºN (Fig. 9c). In general, v-term
315 seems to be the dominant component of subthermocline BTR, but the effect of u-term east of the
316 Mindanao coast is not ignorable.

317 To further clarify which component is dominant on the interannual time scale, the interannual
318 time series of regional mean u-term and v-term are shown in Figure 10. As expected, v-term and
319 u-term exhibit almost opposite interannual variations. v-term is positive during the whole period
320 and is the source of barotropic instability in this region, while u-term is negative for most of the
321 period, implying the zonal flow extracts energy from meso-scale eddies. Moreover, the
322 interannual variation of v-term is consistent with that of BTR (Fig. 7b and Fig. 10), suggesting
323 that the v-term is the dominant component in the interannual variation of BTR. It is worth
324 mentioned that the peak time of v-term is not the same as that of BTR, which is probably due to
325 the modulation of u-term.

326 Above analysis indicates that the interannual modulation of BTR is dominated by v-term,
327 which means the evolution of meridional background flow plays a crucial role in the variation of
328 BTR. East of the Philippine coast, the meridional flow is mainly associated with MC, MUC, and
329 HE (Fig. 1). But in the subsurface layer, the MC south of 15ºN is very weak, while the MUC and
330 HE seem strong (Fig. 1b). Therefore, only HE and MUC are considered in the following
331 discussion.

332 HE is a quasi-permanent anticyclonic eddy that is sustained by two boundary currents, MC
333 and NGCC, and it is also the origin of NECC (e.g., Wyrtki, 1961; Lukas et al. 1991). Both
334 observation and model results reveal that HE tilts northwestward with increasing depth from 3ºN,

130ºE in the surface to the Mindanao coast at about 750 m, as shown in Figure 1 (e.g., Qu et al. 1999; Kashino et al. 1999). Recent studies indicate that the evolution of HE meandering is responsible for the seasonal variation of BTR, which further modulates the EKE variation in both the surface and subsurface layer in this region (Chen et al. 2015; Zhang et al. 2021). Therefore, the interannual evolution of subthermocline BTR east of the Mindanao Island may be also influenced by the subsurface component of HE. To examine the interannual variation of subsurface HE, a box (127º-130.5ºE, 3.5º-8ºN) is chosen to calculate the time series of regional mean HE vorticity in the subsurface layer (Fig. 11a). The result indicates that the interannual variation of HE vorticity exhibits simultaneous correlation with the BTR, and the correlation reaches 0.53. Same as Chen et al. (2015) and Zhang et al. (2021), the enhancement of HE means increasing nonlinear shears of the background flows, which extracts more energy from the mean kinetic energy to EKE through barotropic instability. Thus, we suggest that the interannual variation of subthermocline BTR east of the Mindanao Island (Box 2 in Fig. 4a) is mainly related to the evolution of HE in the subsurface layer.

Further north, the MUC exists below 500 m under the surface MC, which flows northward with a maximum mean velocity around 10 cm/s (Hu and Cui, 1989, 1991). Based on hydrographic data, a time-mean MUC is observed from 6º to 13ºN (e.g., Wang and Hu 1998; Qiu et al. 2015). Nevertheless, in the mean subthermocline circulation derived from OFES outputs (Fig. 1b), the northward velocity between 6º-8ºN is influenced strongly by the HE. Therefore, the following analysis is focused on the meridional velocity between 8º-13ºN to investigate the MUC variations.

EOF analysis is applied to the regional mean meridional velocity time series between 8º-13ºN

357 from coast to 129ºE. Here, the velocity is interpolated onto a regular 20m-depth interval between
358 0-1000 m before the EOF analysis to eliminate the bias caused by irregular vertical grid of model
359 outputs. Figure 12 shows the first two EOF modes and their corresponding PC time series. The
360 first EOF mode captures 69.1 % of the total variance and reveals a surface-intensified pattern that
361 is closely related to MC. Furthermore, the PC1 coincides well with the interannual variation of
362 the MC strength (Fig. 12c), and here the MC strength is defined as the mean velocity from the
363 coast to 129ºE between 8º-13ºN in the upper 460 m. In hence, the first EOF mode reflects the
364 interannual variation of MC. The second EOF mode exhibits subsurface-intensified features of
365 the meridional velocity and accounts for 20.3 % of the total variance. The corresponding PC2
366 agrees well with the interannual variation of MUC strength whose definition is the same as MC
367 but for the depth range of 460-1000 m (Fig. 12d). Similar EOF results are also obtained based on
368 ORAS4 reanalysis data that has a longer period from 1958 to 2017 (not shown). Meanwhile, the
369 interannual variation of MUC matches well with the BTR v-term with a correlation of 0.47 (Fig.
370 10 and Fig. 12d). Therefore, we suggest that the interannual variation of subthermocline BTR
371 east of the Philippine coast is attributed to the evolution of MUC. When the MUC is strong, the
372 nonlinear shear of subthermocline meridional velocity increases and the background flow is more
373 barotropically unstable, which means more kinetic energy of the background currents is
374 converted into the EKE. It is worth noting that the MUC flows northward from the northern part
375 of Box 2 to Box 1 (8º-13ºN, Fig. 1b), exerting significant influences on the subthermocline EKE
376 evolution in both boxes. While the HE exists southeast of Mindanao, and its implication to EKE
377 is mainly in the southern part along the Philippine coast.
378

5. **Discussion**

Both mooring observations and model results reveal the delayed response of subthermocline EKE to ENSO (Fig. 3 and Fig. 4c). Generally, this kind of delayed oceanic response to ENSO is usually associated with the adjustment through baroclinic Rossby waves (e.g., Qiu and Chen 2010; Hsin and Qiu. 2012). Based on the altimeter products, Hsin and Qiu (2012) denotes that the intensity and meridional migration of NECC can be modulated by the westward propagating Rossby wave. As the source region of NECC, HE may be also influenced by Rossby wave. To investigate this impact, the Hovmöller diagrams of sea surface height anomaly (SSHA) between 5º-8ºN derived from satellite altimetry and OFES outputs are shown in Figure 13. The result indicates that OFES outputs capture the observed characteristics of SSHA on both the annual and interannual time scales, which confirms the capability of OFES in simulating the ocean circulation in the Pacific. On the interannual time scale, when El Niño occurs, positive wind stress curl anomaly (WSCA) near the dateline excites negative SSHA, which propagates westward in the form of the first mode baroclinic Rossby wave, affecting the intensity of HE in a delayed fashion (Fig. 11b and Fig. 13). For example, during the 15/16 El Niño event, the negative SSHA appears near the dateline in August 2015, then propagates westward and arrives to the western boundary in February 2016, which is consistent with the peak time of HE's vorticity during this event (Fig. 11b). Therefore, the vorticity of HE exhibits a lag correlation with Nino3.4 index, and the coefficient reaches 0.54 when the Nino3.4 index leads by 5 months (Fig. 11b). Because the interannual variation of subthermocline EKE in Box 2 is modulated by HE through its barotropic instability, the subthermocline EKE in Box 2 lags Nino3.4 index by 8 months (Fig. 6). This 3-month time lag between the HE variation and subthermocline EKE is

supposed to be related to the internal adjustment process of the ocean.

As for the interannual variation of MUC, there are only a few previous studies due to the lack of long-time subsurface observations (e.g., Hu et al., 2016; Ren et al., 2020). Based on 4-year subsurface mooring measurements and numerical sensitivity experiments, Hu et al. (2016) suggests that Rossby waves generated near the dateline are of much significance in the MUC variation. Moreover, the Rossby waves usually take about one year translating from the dateline to the western boundary in the latitude band of 10º-15ºN, which is probably the reason that the MUC and corresponding BTR lag the Nino3.4 index for about one year as shown in Figure 10 and Figure 12d. Furthermore, Qiu et al. (2015) has emphasized the role of baroclinic instability in the eddy generation and Figure 7b also demonstrates the significance of baroclinic instability especially during 2003. In hence, although the barotropic instability is dominant in the interannual variation of subthermocline EKE, the baroclinic instability also has substantial contributions, and detailed investigations are needed in future research.

6. Conclusion

The interannual variation of subthermocline EKE east of the Philippine coast is investigated based on 4-year mooring observations during 2015-2019 and OFES outputs during 1995-2017. The results indicate that the interannual variation of subthermocline EKE is closely related to ENSO. Generally, elevated subthermocline EKE appears after El Niño events, and the correlation between EKE and Nino3.4 index is 0.49 when Nino3.4 index leads by 14 months. Nevertheless, such correlation is not latitudinally uniform: low-latitude subthermocline EKE between 5º-9ºN lags Nino3.4 index by about 8 months, while the delay is 16 months in relatively higher latitudes

between 9º-14ºN. Mooring measurements at 8.5ºN, 130ºE and 12.5ºN, 130ºE also confirm this delayed response. Further investigations imply that the background flow instability including baroclinic and barotropic instability plays an essential role in the interannual modulation of subthermocline EKE, and the barotropic instability is dominant. Furthermore, the barotropic instability is associated with different background currents. In the southern part of the region east of the Philippines, it is in connection with the subsurface component of the quasi-permanent anticyclonic eddy HE. In the northern part, it is closely related to the MUC. Both MUC and HE are modulated by the westward propagating first mode baroclinic Rossby wave excited by the wind stress curl anomalies near the dateline during ENSO events. Therefore, the subthermocline EKE lags the Nino3.4 index, and subthermocline EKE in the southern part responds faster to ENSO than that in the northern part due to the increasing phase speed of the Rossby wave in the lower-latitude region.

Acknowledgments

The authors are grateful to Dr. Cesar Villanoy for helping to recover mooring data. This study is supported by the National Natural Science Foundation of China (No.41776021 and 42122041), the Strategic Priority Research Program of the Chinese Academy of Sciences (No. XDB42010105), the National Key Research and Development Program of China (No.2020YFA0608801 and 2017YFA0603202).

Data Availability Statement

The mooring ADCP data is available at the NPOCE website (http://npoce.qdio.ac.cn/moored), and OFES data is downloaded from the Asia Pacific Data Research Center (APDRC) website.

Reference

Assassi, C., Y. Morel, F. Vandermeirsch, A. Chaigneau, C. Pegliasco, et al., 2016: An Index Distinguish Surface- and Subsurface-Intensified Vortices from Surface Observations. *J. Phys. Oceanogr.*, 46: 2529-2552, http://doi.org/10.1175/JPO-D-15-0122.1.

Chelton, D. B., P. Gaube, M. G. Schlax, J. J. Early, and R. M. Samelson, 2011a: The influence of nonlinear mesoscale eddies on near-surface chlorophyll, *Science*, 334, 328–332. http://doi.org/10.1126/science.1208897

Chelton, D. B., M. G. Schlax, R. M. Samelson, 2011b: Global observations of nonlinear mesoscale eddies, *Prog. Oceanogr.*, 91, 167-216, http://doi.org/10.1016/j.pocean.2011.01.002

Chen, X., B. Qiu, S. M. Chen, Y. Q. Qi, and Y. Du, 2015: Seasonal eddy kinetic energy modulations along the North Equatorial Countercurrent in the western Pacific. *J.Geophys. Res. Oceans.*, 120, 6351–6362, https://doi.org/10.1002/2015JC011054.

Chiang, T. -L., and T. D. Qu, 2013: Subthermocline eddies in the western equatorial Pacific as shown by an eddy-resolving OGCM. *J. Phys. Oceanogr.*, 43, 1241–1253, https://doi.org/10.1175/JPO-D-12-0187.1.

Chiang, T. -L., C. R. Wu, T. D. Qu, and Y. C. Hsin, 2015: Activities of 50–80 day subthermocline eddies near the Philippine coast. *J. Geophys. Res. Oceans.*, 120, 3606–3623, https://doi.org/10.1002/2013JC009626

Dutrieux, P., 2009: Tropical western Pacific currents and the origin of intraseasonal variability below the thermocline. Ph.D. thesis, University of Hawaii at Manoa, 140 pp.

Faghmous J. H., I. Frenger, Y. Yao, R. Warmka, A. Lindell, et al., 2015: A daily global mesoscale ocean eddy dataset from satellite altimetry. *Sci Data*, 2:150028.

http://doi.org/10.1038/sdata.2015.28

Firing, E., Y. Kashino, and P. Hacker, 2005: Energetic subthermocline currents observed east of Mindanao. *Deep-Sea Res. II*, 52, 605–613, https://doi.org/10.1016/j.dsr2.2004.12.007.

Fu, L. -L., 2009: Pattern and velocity of propagation of the global ocean eddy variability, *J. Geophys. Res.*, 114, C11017, http://doi.org/10.1029/2009JC005349.

Hsin, Y. -C., and B. Qiu, 2012: Seasonal fluctuations of the surface North Equatorial Countercurrent (NECC) across the Pacific basin, *J. Geophys. Res.*, 117, C06001, https://doi.org/10.1029/2011JC007794

Hu D. X. and Coauthors, 2020: Review on observational studies of western tropical Pacific Ocean circulation and climate. *J. Ocean. Limnol.*, 38, 906–929, https://doi.org/10.1007/s00343-020-0240-1.

Hu, D. X., and M. C. Cui, 1989: The western boundary current in the far-western Pacific Ocean, *in Proceedings of Western International Meeting and Workshop on TOGA COARE*, edited by J. Picaut, R. Lukas, and T. Delcroix, pp. 123–134, Inst. Fr. de Rech. Sci. pour le Deev. en Coop., Noumeea.

Hu, D. X., and M. C. Cui, 1991: The western boundary current of the Pacific and its role in the climate. *Chin. J. Oceanol. Limnol.*, 9, 1–14, https://doi.org/10.1007/BF02849784.

Hu, D., and Coauthors, 2015: Pacific western boundary currents and their roles in climate. *Nature*, 522(7556), 299–308. https://doi.org/10.1038/nature14504

Hu, S. J., D. X. Hu, C. Guan, F. Wang, L. L. Zhang,F. J. Wang and Q. Y. Wang, 2016: Interannual Variability of the Mindanao Current/Undercurrent in Direct Observations and Numerical Simulations. *J. Phys. Oceanogr.*, 46 641 (2), 483-499.

http://doi.org/10.1175/jpo-d-15-0092.1.

Johnson, G. C., and K. E. McTaggart, 2010: Equatorial Pacific 13ºC Water eddies in the eastern subtropical South Pacific Ocean. *J. Phys. Oceanogr.*, 40, 226–236. https://doi.org/10.1175/2009JPO4287.1

Kashino, Y., H. Watanabe, B. Herunadi, M. Aoyama, and D. Hartoyo, 1999: Current variability at the Pacific entrance of the Indonesian throughflow. *J. Geophys. Res.*, 104, 11021–11035, https://doi.org/10.1029/1999JC900033

Kashino, Y., N. Espana, F. Syamsudin, K. Richards, T. Jensen, P. Dutrieux, and A. Ishida, 2009: Observations of the North Equatorial Current, Mindanao Current, and Kuroshio Current System during the 2006/07 El Niño and 2007/08 La Niña, *J. Oceanogr.*, 65(3), 325–333, http://doi.org/10.1007/s10872-009-0030-z.

Lukas, R., E. Firing, P. Hacker, P. L. Richardson, C. A. Collins, R. Fine, and R. Gammon, 1991: Observations of the Mindanao Current during the Western Equatorial Pacific Ocean Circulation Study, *J. Geophys. Res.*, 96(C4), 7089–7104, http://doi.org/10.1029/91JC00062

Lukas, R., T. Yamagata, and J. P. McCreary, 1996: Pacific low latitude western boundary currents and the Indonesian throughflow. *J. Geophys. Res.*, 101, 12209–12216, https://doi.org/10.1029/96JC01204.

Masumoto, Y., and Coauthors, 2004: A fifty-year eddy resolving simulation of the world ocean–Preliminary outcomes of OFES (OGCM for the Earth Simulator), *J. Earth Simul.*, 1, 35–56.

McWilliams, J. C., 1985: Submesoscale coherent vortices in the ocean, *Rev. Geophys.*, 23, 165–182, http://doi.org/10.1029/RG023i002p00165

512 Nan, F., F. Yu, C. J. Wei, Q. Ren, and C. H. Fan, 2017: Observations of an extra-large subsurface
513 anticyclonic eddy in the northwestern Pacific subtropical gyre. *J. Mar. Sci. Res. Dev.*, 7, 235,
514 https://doi.org/10.4172/2155-9910.1000234.
515 Nan, F., F. Yu, Q. Ren, C. J. Wei, Y. S. Liu, and S. H. Sun, 2019: Isopycnal mixing of
516 interhemispheric intermediate waters by subthermocline eddies east of the Philippines. *Sci.*
517 *Rep.*, 9, 2957, http://doi.org/10.1038/s41598-019-39596-2
518 Nitani, H., 1972: Beginning of the Kuroshio. In H. Stommel, and K. Yoshida (Eds.), Kuroshio:
519 Physical aspects of the Japan current (pp. 129-163). Seattle, WA: University of Washington
520 Press.
521 Qiu, B., 1999: Seasonal eddy field modulation of the North Pacific Subtropical Countercurrent:
522 TOPEX/Poseidon observations and theory. *J. Phys. Oceanogr.*, 29, 2471–2486,
523 https://doi.org/10.1175/1520-0485(1999)029,2471:SEFMOT.2.0.CO;2.
524 Qiu, B., and S. M. Chen, 2010: Interannual-to-decadal variability in the bifurcation of the North
525 Equatorial Current off the Philippines. *J. Phys. Oceanogr.*, 40, 213–225,
526 http://doi.org/10.1175/2010JPO4462.1
527 Qiu, B., D. L. Rudnick, S. Chen, and Y. Kashino, 2013: Quasistationary North Equatorial
528 Undercurrent jets across the tropical North Pacific Ocean, *Geophys. Res. Lett.*, 40,
529 2183–2187, http://doi.org/10.1002/grl.50394.
530 Qiu, B., S. M. Chen, D. L. Rudnick and Y. J. Kashino, 2015: A New Paradigm for the North
531 Pacific Subthermocline Low-Latitude Western Boundary Current System, *J. Phys.*
532 *Oceanogr.*,45, 2407-2423, http://doi.org/10.1175/JPO-D-15-0035.1
533 Qu T. D., H. Mitsudera, and T. Yamagata, 1999: A climatology of the circulation and water mass

distribution near the Philippine coast. *J. Phys. Oceanogr.*, 29, 1488–1505, https://doi.org/10.1175/1520-0485(1999)029,1488:ACOTCA.2.0.CO;2.

Qu T. D., T. L. Chiang, C. R. Wu, P. Dutrieux, and D. X. Hu, 2012: Mindanao current/undercurrent in an eddy-resolving GCM. *J. Geophys. Res.*, 117, C06026, https://doi.org/10.1029/2011JC007838.

Ren Q. P., Y. L. Li, F. Wang, J. Duan, S. J. Hu, and F. J. Wang, 2020: Variability of the Mindanao Current Induced by El Niño Events, *J. Phys. Oceanogr.*, http://doi.org/10.1175/JPO-D-19-0150.1.

Richardson, P. L., A. S. Bower, and W. Zenk, 2000: A census of Meddies tracked by floats. *Prog. Oceanogr.*, 45, 209–250, http://doi.org/10.1016/S0079-6611(99)00053-1.

Sasaki, H., M. Nonaka, Y. Masumoto, Y. Sasai, H. Uehara, and H. Sakuma, 2008: An eddy-resolving hindcast simulation of the quasiglobal ocean from 1950 to 2003 on the Earth Simulator, *High Resolution Numerical Modeling of the Atmosphere and Ocean*, K. Hamilton and W. Ohfuchi, Eds. Springer, 57–185, http://doi.org/10.1007/978-0-387–49791-4_10.

Shapiro, G. I., and S. L. Meschanov, 1991: Distribution and spreading of Red Sea Water and salt lens formation in the northwest Indian Ocean. *Deep-Sea Res.*, 38A, 21–34, http://doi.org/10.1016/0198-0149(91)90052-H.

Simpson, J. J., and R. J. Lynn, 1990: A mesoscale eddy dipole in the offshore California Current. *J. Geophys. Res.*, 95 (C8), 13 009–13 022. https://doi.org/10.1029/JC095iC08p13009

Song L. N., Y. L. Li, C. Y. Liu, and F. Wang, 2016: Subthermocline anticyclonic gyre east of Mindanao and its relationship with the Mindanao Undercurrent, *Chinese Journal of Oceanology and Limnology*, 35(6), 1303-1318, https://doi.org/10.1007/s00343-017-6111-8

556 Stammer, D., 1998: On eddy characteristics, eddy transports, and mean flow properties, *J. Phys.*
557 *Oceanogr.*, 28, 727–739.
558 http://doi.org/10.1175/1520-0485(1998)028<0727:OECETA>2.0.CO;2
559 Toole, J. M., R. C. Millard, Z. Wang, and S. Pu, 1990: Observations of the Pacific North
560 Equatorial Current Bifurcation at the Philippine Coast. *J. Phys. Oceanogr.* 20, 307-318,
561 http://doi.org/10.1175/1520-0485(1990)020<0307:OOTPNE>2.0.CO;2.
562 Wang F, Zang N, Li Y L, Hu D X. 2015. On the subsurface countercurrents in the Philippine Sea.
563 J . Geophys . Res . Oceans , 120 (1): 131-144.
564 Wang, F., and D. X. Hu, 1998: Dynamic and thermohaline properties of the Mindanao
565 undercurrent, part I: Dynamic structure, *Chin. J. Oceanol.*, 16(2):122-127,
566 http://doi.org/10.1007/BF02845177
567 Wang, Q. Y., F. G. Zhai, F. J. Wang, and D. X. Hu, 2014: Intraseasonal variability of the
568 subthermocline current east of Mindanao. J. Geophys. Res. Oceans, 119, 8552–8566,
569 https://doi.org/10.1002/2014JC010343.
570 Wyrtki, K., 1961: Physical oceanography of the southeast Asian waters. NAGA Rep. 2, Scripps
571 Institution of Oceanography, 195 pp., https://escholarship.org/uc/item/49n9x3t4.
572 Xu, A. Q., F. Yu, and F. Nan, 2019: Study of subsurface eddy properties in northwestern Pacific
573 Ocean based on an eddy-resolving OGCM. *Ocean. Dyn.*, 69, 463–474,
574 https://doi.org/10.1007/s10236-019-01255-5.
575 Yuan, D., Z. Zhang, P. C. Chu, and W. K. Dewar, 2014: Geostrophic circulation in the tropical
576 north Pacific Ocean based on Argo profiles. *J. Phys. Oceanogr.*, 44, 558–575,
577 https://doi.org/10.1175/JPO-D-12-0230.1.

578 Zhang L. L., Y. C. Hui, T. D. Qu, and D. X. Hu, 2021: Seasonal variability of subthermocline eddy
579 kinetic energy east of the Philippines, *J. Phys. Oceanogr.*,
580 http://doi.org/10.1175/JPO-D-20-0101.1.
581 Zhang, L. L., D. X. Hu, S. J. Hu, F. Wang, F. J. Wang, and D. L. Yuan, 2014: Mindanao
582 Current/Undercurrent measured by a subsurface mooring,. *J. Geophys. Res.*, 119, 3617–3628,
583 https://doi.org/10.1002/2013JC009693.
584
585
586
587
588
589
590
591
592
593
594
595
596

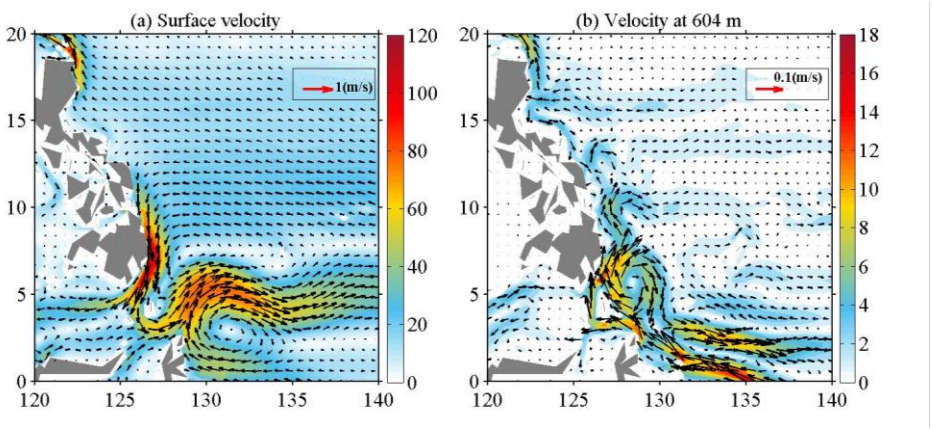

Fig. 1. (a) Surface (2.5 m) and (b) subsurface (604 m) climatological mean velocity (vectors; m/s) derived from OFES during 1995 to 2017. Shadings denote the magnitude of the velocity.

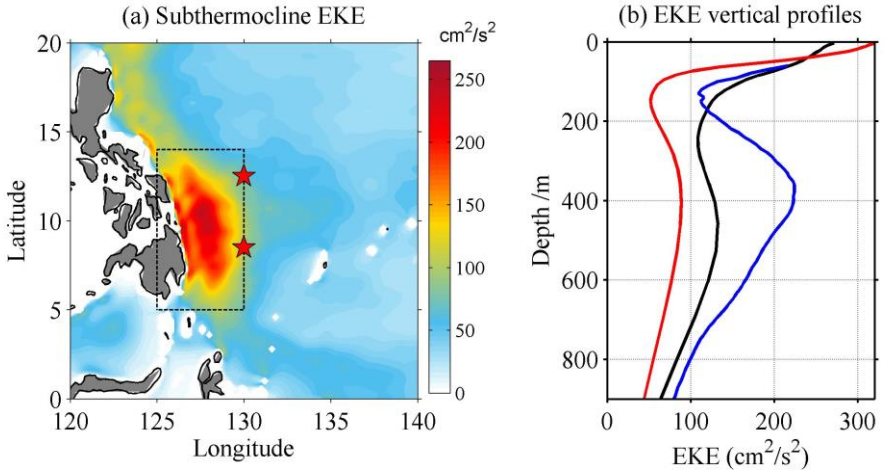

Fig. 2. (a) All-time mean subthermocline EKE (300-700 m; cm^2/s^2) calculated with 150-day high-pass-filtered velocity from OFES during 1995-2017. (b) EKE profiles calculated with velocity from OFES (red) and mooring ADCP (blue) at 8.5ºN, 130ºE during December 2015 to August 2019, and the regional (125º-130ºE, 5º-14ºN) mean profile calculated with OFES during 1995-2017 (black). Red stars in (a) indicate the mooring locations at 8.5ºN, 130ºE and 12.5ºN, 130ºE.

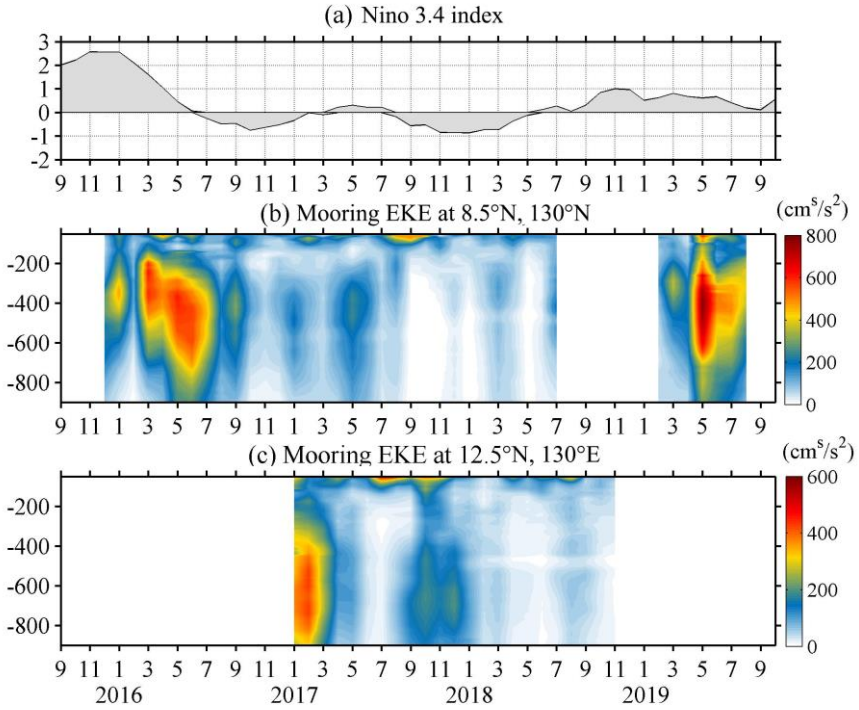

610

611 Fig. 3. (a) Nino 3.4 index, and monthly time series of EKE (color) derived from mooring

612 measurements at (b) 8.5ºN, 130ºE and (c) 12.5ºN, 130ºE during September 2015 to October 2019.

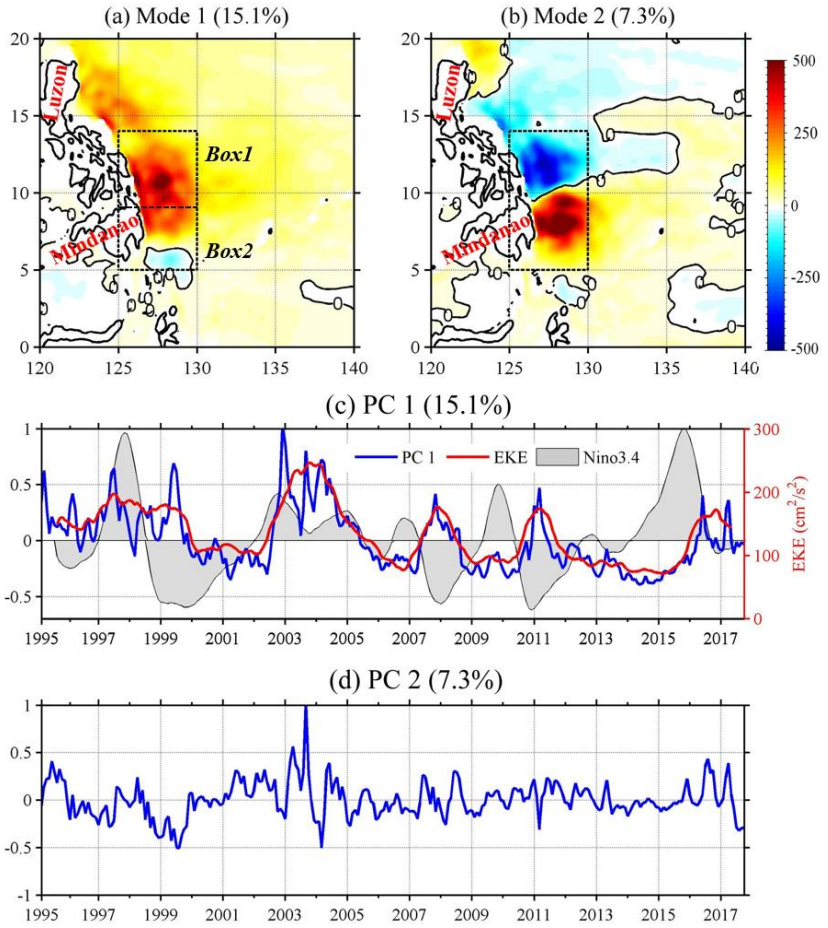

Fig. 4. (a) Spatial pattern and (c) primary component of the first EOF mode of monthly subthemrocline EKE (300-700 m) in the western Pacific derived from OFES during 1995 to 2017. (b) and (d) are the same as (a) and (c), but for the second EOF mode. The red curve and grey shading in (c) are the regional (5º-14ºN, 125º-130ºE) mean time series of subthermocline EKE and normalized Nino 3.4 index, respectively, and both curves have been smoothed with a one-year low-pass filter.

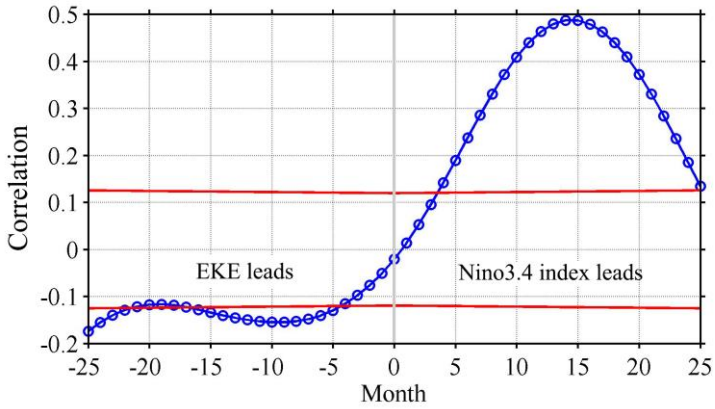

Fig. 5. Lead-lag correlation between the regional mean subthermocline EKE (red curve in Fig. 4c) and Nino 3.4 index (grey coloring in Fig. 4c). Positive lag means Nino 3.4 index leads the EKE.

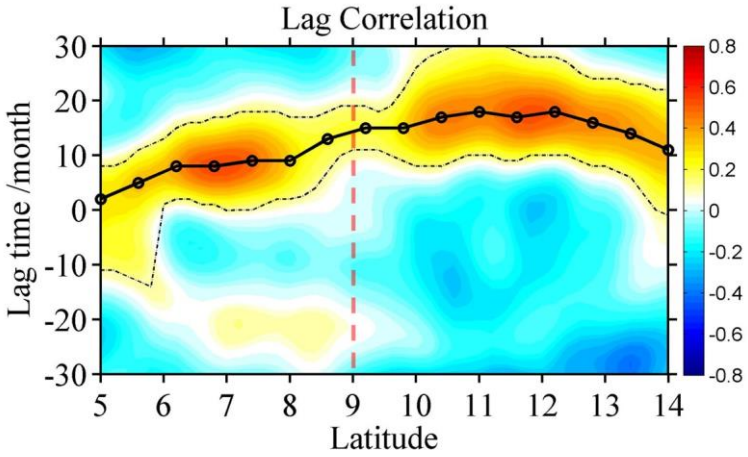

Fig. 6. Lead-lag correlation between Nino3.4 index and zonal mean (125º-130ºE) subthermocline EKE (300-700 m) east of the Philippine coast at different latitudes. Positive lag means Nino 3.4 index leads the EKE.

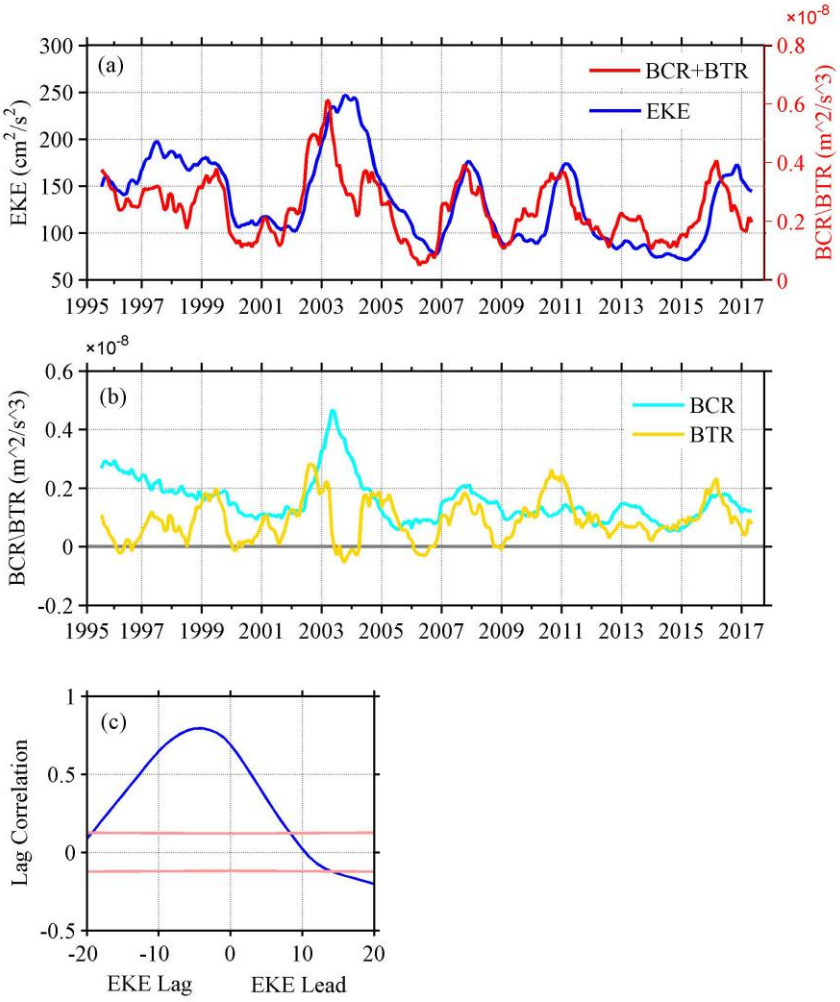

631

632 Fig. 7. (a) Time series of the regional (5º-14ºN, 125º-130ºE) mean subthermocline EKE (red) and
633 the sum of BTR and BCR (blue). (b) is the same as (a), but for the BTR (yellow) and BCR (light
634 blue). (c) denotes the lead-lag correlation between the red and blue curves in (a). All the time
635 series are derived from OFES during 1995-2017 and smoothed with a one-year low-pass filter.

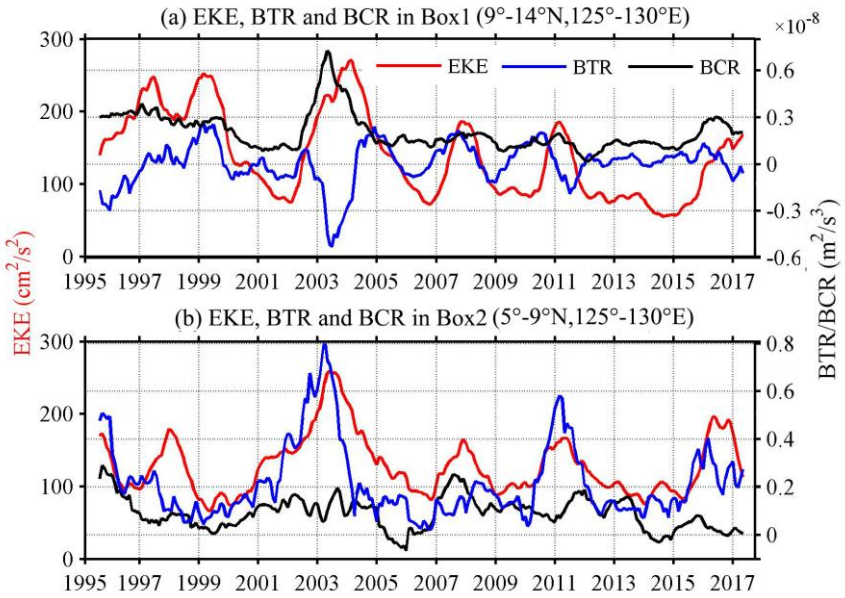

636

637 Fig. 8. (a) Time series of the regional mean subthermocline EKE (red), BTR (blue) and BCR
638 (black) in Box1 (9º-14ºN, 125º-130ºE). (b) is the same as (a), but for Box 2 (5º-9ºN, 125º-130ºE).
639 All the time series are derived from OFES during 1995-2017 and smoothed with a one-year
640 low-pass filter.

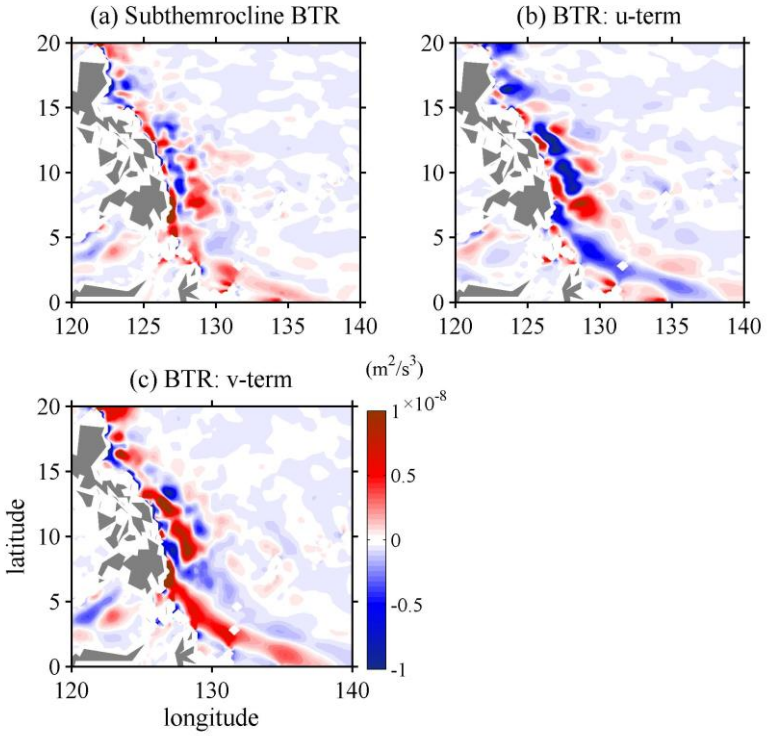

641

642 Fig. 9. (a) Climatological mean BTR in the subthermocline layer (300–700 m) derived from OFES
643 during 1995-2017. (b) and (c) are the same as (a), but for the u-term and v-term, respectively.

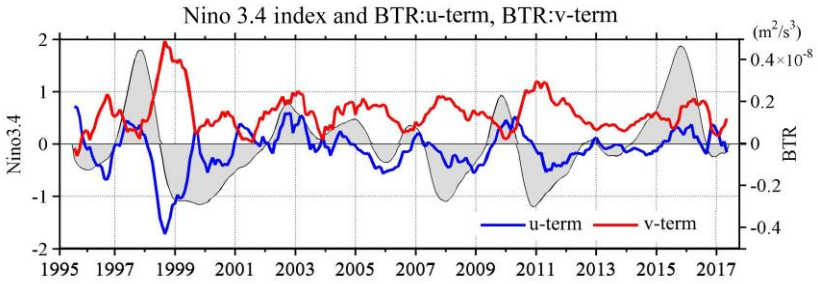

644

645 Fig. 10. Time series of the regional (125º-130ºE, 5º-14ºN) mean BTR u-term (blue) and v-term
646 (red) in the subthermocline layer (300-700 m) derived from OFES during 1995-2017. Grey bars
647 denote the Nino3.4 index. All the time series have been smoothed with a one-year low-pass filter.

648

649

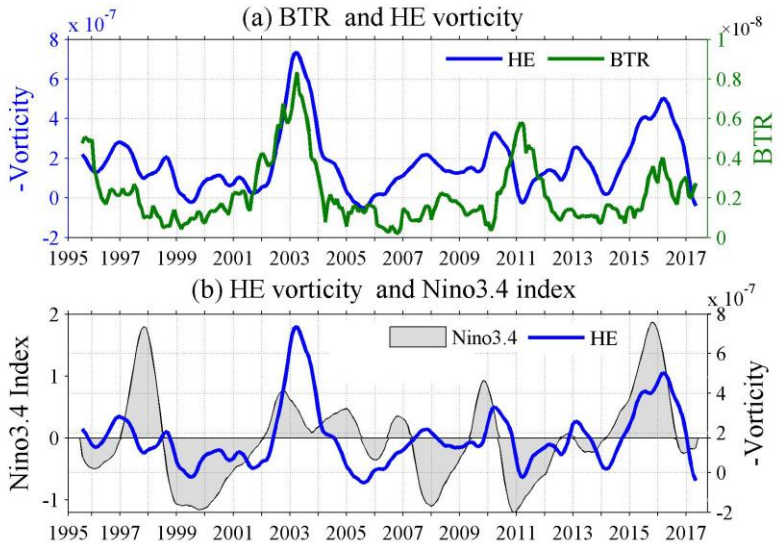

650

651 Fig. 11. (a) Time series of the regional mean BTR (green; 5º-9ºN, 125º-130ºE) and HE vorticity
652 (blue; 3.5º-8ºN, 127º-130.5ºE) in the subthermocline layer (300-700 m) derived from OFES
653 during 1995-2017. (b) Grey bars denote the Nino3.4 index, and blue curve is the same as that in
654 (a). All the time series have been smoothed with a one-year low-pass filter.

655

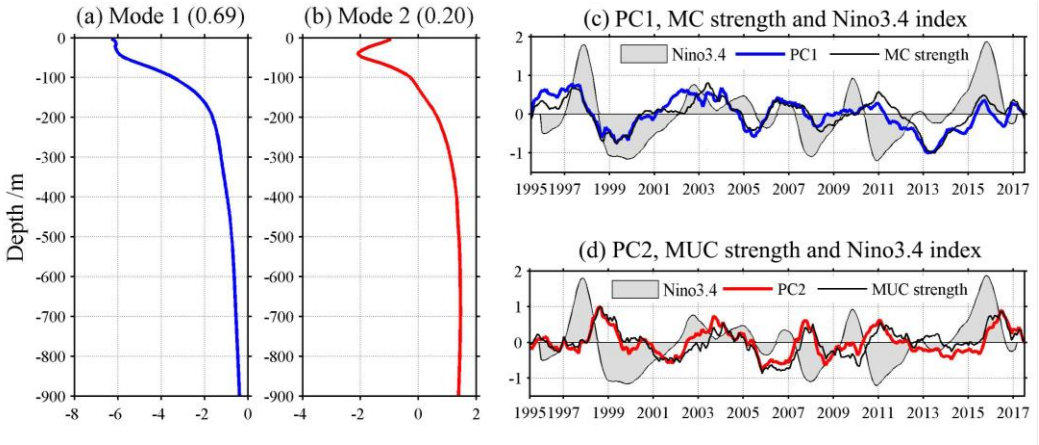

Fig. 12. (a) Vertical profile and (c) primary component of the first EOF mode of monthly meridional velocity averaged in 8º-13ºN, 126º-129ºE from OFES during 1995-2017. (b) and (d) are the same as (a) and (c), but for the second EOF mode. Grey bars in (c) and (d) denote the time series of Nino 3.4 index. Black curves in (c) and (d) indicate the MC and MUC strength, respectively. Here the MC strength is defined as the normalized mean velocity from 126ºE to 129ºE between 8º-13ºN in the upper 460 m, and the definition of MUC strength is the same as the MC, but for the depth range of 460-1000 m.

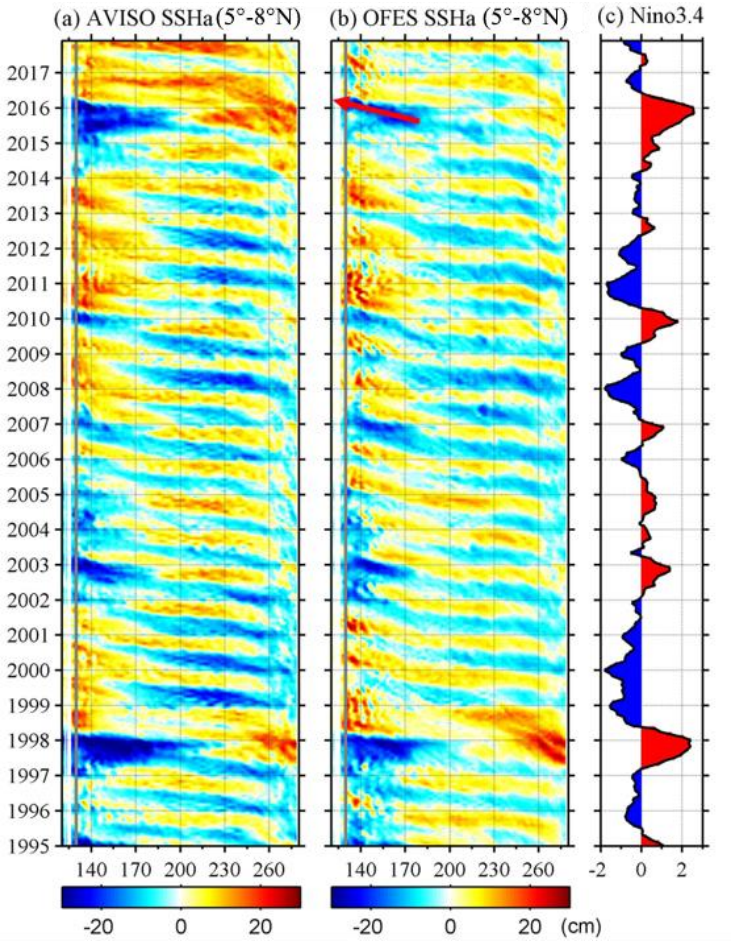

665

666 Fig. 13. Time-longitude plots of monthly sea surface height anomalies averaged between 5º-8ºN

667 from (a) satellite alimtetry and (b) OFES outputs. (c) Nino 3.4 index.